

Precise orbit determination for BDS3 experimental satellites using iGMAS and MGEX tracking networks

Xingxing Li^{1,2} · Yongqiang Yuan¹ · Yiting Zhu¹ · Jiande Huang¹ · Jiaqi Wu¹ · Yun Xiong¹ · Xiaohong Zhang¹ · Xin Li¹

Received: 8 November 2017 / Accepted: 6 April 2018 / Published online: 21 April 2018
© Springer-Verlag GmbH Germany, part of Springer Nature 2018

Abstract

In this contribution, we focus on the precise orbit determination (POD) for BDS3 experimental satellites with the international GNSS Monitoring and Assessment System (iGMAS) and Multi-GNSS Experiment (MGEX) tracking networks. The datasets of DOY (day of year) 001–230 in 2017 are analyzed with different processing strategies. By comparing receiver clock biases and receiver B1I–B3I DCBs, it is confirmed that there is no obvious systematic bias between experimental BDS3 and BDS2 in the common B1I and B3I signals, which indicates that experimental BDS3 and BDS2 can be treated as one system when performing combined POD. With iGMAS-only BDS3 stations, the 24-h overlap RMS of BDS3 + BDS2 + GPS combined POD is 24.3, 16.1 and 8.4 cm in along-track, cross-track and radial components, which is better than BDS3-only POD by 80–90% and better than BDS3 + BDS2 combined POD by about 10%. With more stations (totally 20 stations from both iGMAS and MGEX) and the proper ambiguity resolution strategy (GEO ambiguities are float and BDS3 ambiguities are fixed), the performance of BDS3 POD can be further improved to 14.6, 7.9 and 3.7 cm, respectively, in along-track, cross-track and radial components, which is comparable to the performance of BDS2 POD. The 230-day SLR validations of C32, C33 and C34 show that the mean differences of –3.48, 7.81 and 8.19 cm can be achieved, while the STD is 13.35, 13.46 and 13.11 cm, respectively. Furthermore, the 230-day overlap comparisons reveal that C31 most likely still uses an orbit-normal mode and exhibits similar orbit modeling problems in orbit-normal periods as found in most of the BDS2 satellites.

Keywords Precise orbit determination · BDS3 and BDS2 · Multi-GNSS experiment (MGEX) · iGMAS · Ambiguity resolution · Inter-system bias · Attitude mode

1 Introduction

The development of Chinese BeiDou navigation satellite system can be divided into three phases. The first phase is the BeiDou Satellite Navigation Experimental system (BDS1), which has been completed in 2003. Following the operation of BDS1, China started the construction of regional BeiDou system (BDS2). By the end of 2012, the BDS2 has been providing regional positioning, navigation and timing (PNT) services for the users throughout the Asia-Pacific region with a constellation of five Geostationary Earth Orbits

(GEOS), five Inclined Geosynchronous Orbits (IGSOs) and four Medium altitude Earth Orbit (MEO) satellites. In 2015, China started the construction of a global BeiDou system (BDS3; SCIO 2016). By October 2017, five experimental BDS3 satellites have been launched. It is expected to provide global service with 5 GEO, 3 IGSO and 27 MEO satellites by 2020. In Table 1, the basic status of BDS satellites is listed. For brevity, the BDS3 henceforth refers to these five experimental BDS3 satellites in this paper.

The rapid development of the BDS2 satellite system has brought widespread interest in the field of GNSS, and a series of studies have been carried out on precise orbit determination (POD) of BDS2 satellites. Several researchers provided initial results of BDS2 POD with BETS (Shi et al. 2012; Zhao et al. 2013; He et al. 2013) and CONGO (Steigenberger et al. 2013) networks. With the development of the IGS Multi-GNSS Experiment (MGEX) network, the model, algorithm and performance of BDS2 POD and precise posi-

✉ Xingxing Li
lxlq109121@gmail.com

¹ School of Geodesy and Geomatics, Wuhan University, 129 Luoyu Road, Wuhan 430079, Hubei, China

² German Research Centre for Geosciences (GFZ), Telegrafenberg, 14473 Potsdam, Germany

Table 1 Satellite status of the BeiDou

Satellite	SVN	Int. sat. ID	NORAD ID	PRN	Notes
BeiDou M1	C001	2007-011A	31115	C30	Decommissioned
BeiDou G2	C002	2009-018A	34779	n/a	Inactive; uncontrolled
BeiDou G1	C003	2010-001A	36287	C01	140.0° E
BeiDou G3	C004	2010-024A	36590	C03	110.5° (moved from 84.0° to new position between Nov 7 and 22, 2012)
BeiDou G4	C006	2010-057A	37210	C04	160.0° E
BeiDou IGSO 1	C005	2010-036A	36828	C06	~ 122° E
BeiDou IGSO 2	C007	2010-068A	37256	C07	~ 119° E
BeiDou IGSO 3	C008	2011-013A	37384	C08	~ 120° E
BeiDou IGSO 4	C009	2011-038A	37763	C09	~ 96.5° E
BeiDou IGSO 5	C010	2011-073A	37948	C10	~ 92.5° E
BeiDou G5	C011	2012-008A	38091	C05	58.75° E
BeiDou M3	C012	2012-018A	38250	C11	Slot A-7
BeiDou M4	C013	2012-018B	38251	C12	Slot A-8
BeiDou M5	C014	2012-050A	38774	C13	Slot B-3; End of signal transmission 21 Oct. 2014
BeiDou M6	C015	2012-050B	38775	C14	Slot B-4
BeiDou G6	C016	2012-059A	38953	C02	80.3°E
BeiDou IGSO 6	C017	2016-021A	41434	C15/C13	~ 95° E; launched 2016/03/29; PRN switch from C15 to C13 on 2016/10/11
BeiDou G7	C018	2016-037A	41586	C17	launched 2016/06/12
BeiDou I1-S	C101	2015-019A	40549	C31	launched 30 March 2017
BeiDou M1-S	C102	2015-037B	40749	C33	Slot A-1, launched 30 July 2015
BeiDou M2-S	C103	2015-037A	40748	C34	Slot A-6, launched 30 July 2015
BeiDou I2-S	C104	2015-053A	40938	C32	launched 29 September 2015
BeiDou M3-S	C105	2016-006A	41315	C35	Slot B-1; launched 1 February 2016

tioning were further investigated (Lou et al. 2014; Li et al. 2015; Zhang et al. 2015; Lou et al. 2016). Several MGEX Analysis Centers (ACs) have been providing precise orbit and clock products of BDS2 satellites (<ftp://cddis.gsfc.nasa.gov/pub/gps/products/mgex>). Among others, the assessment of precise orbit and clock products for different MGEX ACs was carried out by Guo et al. (2016a,b).

For BDS2 GEO satellites, the orbit-normal (ON) attitude mode is applied instead of the Yaw-steering (YS) attitude mode which is usually used for other satellite systems such as GPS, GLONASS and Galileo. Most BDS2 IGSO and MEO satellites switch their attitude mode depending on the angle between the Sun and the orbital plane (usually denoted as β) (Guo 2014; Montenbruck et al. 2015; Dai et al. 2015). The orbit accuracy decreases significantly during and after the attitude mode switch (Lou et al. 2014; Guo et al. 2017). Another special problem for BDS2 is the so-called satellite-induced code bias, which was identified to exist in BDS2 code observations (Wanninger and Beer 2015). The satellite-induced code bias will affect the precision and consistence of the wide-lane ambiguity (Li et al. 2017). By correcting the satellite-induced code bias, the fixing rates of double-

differenced wide-lane ambiguities for BDS2 IGSO and MEO satellites can be improved (Geng et al. 2017).

For the new-generation BDS3 satellites, new signals, satellite attitude mode and atomic clocks have been applied. The experimental BDS3 transmits signals on five frequencies, including backward-compatible B1I (1561.098 MHz) and B3I (1268.52 MHz), and new B1C (1575.42 MHz), B2a (1176.45 MHz), B2b (1207.14 MHz) (Zhao et al. 2017; CSNO 2017). The B3I signal of the experimental BDS3 satellites is modulated by binary phase shift keying (BPSK), which is in accordance with BDS2 (Zhang et al. 2017a; CSNO 2018). The under constructing global BDS3 satellites will continue it for backward compatibility with BDS2. The B3 band is intended for authorized use only in the global stage of BDS (Yang et al. 2017; Kaplan and Hegarty 2017). Zhang et al. (2017a) presented initial assessment of experimental BDS3 satellite observations. The results revealed that the observational quality of experimental BDS3 is comparable to that of GPS and Galileo for their employed receivers. In addition, the satellite-induced code bias is proved to be absent in code observations of experimental BDS3 satellites. Tan et al. (2016) processed the data of 35 days from 9 iGMAS

Table 2 iGMAS experimental BDS3 tracking stations (stations with GNSS_GGR receivers are excluded)

Site name	Receiver	Antenna	Location
BJF1	CETC-54-GMR-4016 SW-Version1.0	LEIAR25.R4 LEIT	(39°N, 115°E)
BRCH	CETC-54-GMR-4016 SW-Version1.0	NOV750.R4 NOVS	(52°N, 10°E)
CANB	CETC-54-GMR-4011 SW-Version1.0	GNSS-750	(35°S, 149°E)
DWIN	CETC-54-GMR-4011 SW-Version1.0	GNSS-750	(14°S, 132°E)
KNDY	CETC-54-GMR-4016 SW-Version1.0	GNSS-750	(7°N, 80°E)
LHA1	CETC-54-GMR-4016 SW-Version1.0	NOV750.R4 NOVS	(29°N, 91°E)
PETH	CETC-54-GMR-4011 SW-Version1.0	GNSS-750	(29°S, 115°E)
WUH1	CETC-54-GMR-4016 SW-Version1.0	LEIAR25.R4 LEIT	(30°N, 114°E)
ZHON	CETC-54-GMR-4011 SW-Version1.0	GNSS-750	(69°S, 76°E)
CLGY	CETC-54-GMR-4016 SW-Version1.0	LEIAR25.R4 LEIT	(51°N, 115°W)

(the international GNSS Monitoring and Assessment System) stations for experimental BDS3 POD, and the overlap RMS for experimental BDS3 IGSO and MEO satellites is approximately 10 and 40 cm in the radial component. Xie et al. (2017) used 11 stations to conduct experimental BDS3 POD for 16 days, and the overlap precision in the radial component is 6–14 cm. The accuracy of experimental BDS3 POD is still much worse than BDS2 satellites due to the limited tracking stations.

The International GNSS Service (IGS) has initiated the MGEX project in 2012 to collect and analyze data of emerging new signals and systems (Montenbruck et al. 2017). The MGEX network began to provide BDS observations data in 2013. At the moment, more than 160 stations can track BDS2 satellites. The iGMAS tracking network is developed by China to collect multi-GNSS observations and provide satellite orbit and clock, station coordinates and kinds of products for global users (Cai et al. 2016). Until now, the iGMAS network consists of 23 stations, and all of the stations support the BDS2 signal tracking. More than 180 iGMAS/MGEX stations are tracking the BDS2 satellites. As for experimental BDS3, their B1I and B3I signals are continuously tracked by 26 stations, including 16 iGMAS stations equipped with CETC-54-GMR-4011/4016 or GNSS_GGR receivers as well as 10 MGEX stations equipped with SEPT POLARX5 5.1.1 or higher version receivers.

In this contribution, we focus on evaluating the POD performance of BDS3 experimental satellites with the iGMAS and MGEX networks. The paper is organized as follows. After this introduction, BDS3 tracking networks are characterized in Sect. 2. In Sect. 3, the models for BDS3 POD are formulated, and different POD strategies are designed to investigate BDS3 POD. In Sect. 4, observations of DOY001–230 are processed, and the BDS3 POD performances are evaluated, followed by the SLR validation in Sect. 5. The attitude of BDS3 experimental satellites is briefly discussed in Sect. 6, and the conclusions are summarized in Sect. 7.

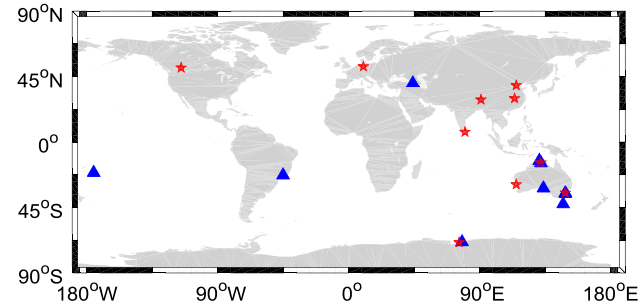


Fig. 1 Distribution of experimental BDS3 tracking stations from iGMAS (the red stars) and MGEX (the blue triangles)

2 Tracking networks for BDS3 experimental satellites

By July 2017, there are 16 iGMAS stations that can track the backward-compatible B1I and B3I signals of experimental BDS3. However, six of them, namely ABJA, CHU1, GUA1, HMNS, THAT and XIA1, equipped with GNSS_GGR receivers, present numerous outliers and problematic observations, and thus are not employed in this contribution. The details of the rest ten iGMAS tracking stations are summarized in Table 2, and their distribution is shown in Fig. 1 (red stars). It is worth noticing that most of these stations are located in China and Australia, while only two stations are in Europe and North America.

By July 2017, there are more than 130 MGEX stations tracking BDS2, among which 31 stations are capable of tracking BDS2 B1I B2I B3I signals. The distribution of these triple-frequency BDS2 stations is shown in Fig. 3 in red triangles. Ten MGEX stations with SEPT POLARX5 receivers provide the backward-compatible B1I and B3I dual-frequency observations of experimental BDS3. Most of these stations are located in Australian area, as shown in Fig. 1. The detailed information of these MGEX BDS3 stations is listed in Table 3.

Table 3 MGEX experimental BDS3 tracking stations

Site name	Receiver	Antenna	Location
ARUC	SEPT POLARX5 5.1.2	ASH701945C_M SCIS	(40°N, 44°E)
CEDU	SEPT POLARX5 5.10	AOAD/M_T NONE	(32°S, 133°E)
CHPI	SEPT POLARX5 5.1.1	TPSCR.G3 NONE	(23°S, 45°W)
DARW	SEPT POLARX5 5.10	JAVRINGANT_DM NONE	(13°S, 131°E)
DAV1	SEPT POLARX5 5.1.1	LEIAR25.R3 LEIT	(69°S, 78°E)
HOB2	SEPT POLARX5 5.10	AOAD/M_T NONE	(43°S, 147°E)
KAT1	SEPT POLARX5 5.1.1	LEIAR25.R3 LEIT	(14°S, 132°E)
STR1	SEPT POLARX5 5.10	ASH701945C_M NONE	(35°S, 149°E)
TID1	SEPT POLARX5 5.1.1	AOAD/M_T NONE	(35°S, 149°E)
TONG	SEPT POLARX5 5.1.2	TRM59800.00 NONE	(21°S, 175°W)

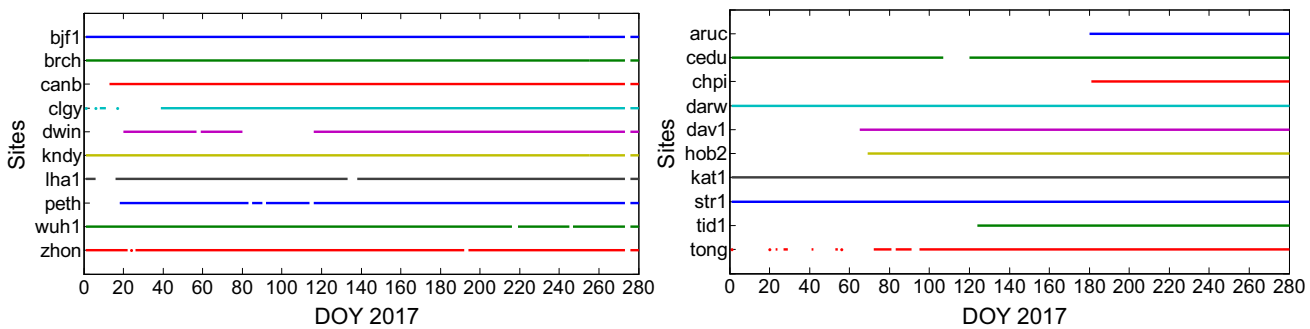


Fig. 2 Availability of experimental BDS3 dual-frequency observations at iGMAS (left panel) and MGEX (right panel) stations

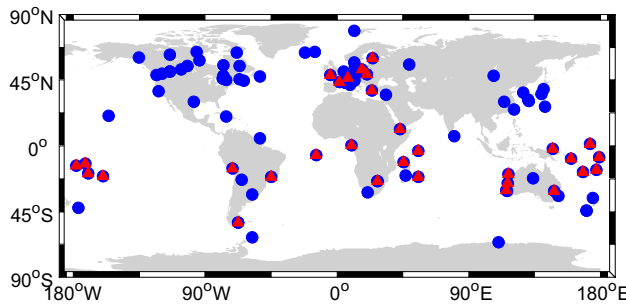


Fig. 3 Distribution of the selected stations for BDS2 and GPS. The red triangles indicate the stations with triple-frequency BDS2 tracking ability, and the blue circles are stations for GPS

The availability of experimental BDS3 dual-frequency observations at the ten iGMAS and ten MGEX stations is shown in Fig. 2, for DOY001-280 of 2017. It is easy to figure out that most iGMAS stations are capable of providing continuous BDS3 observations. As for the MGEX stations, only four of them provide continuous BDS3 observations in the first 70 days. The continuous BDS3 observations at ARUC and CHPI are not available before DOY180. Totally 20 stations can provide BDS3 dual-frequency observations after DOY180. Besides, 67 GPS stations (marked as blue circles in Fig. 3) are also selected here for BDS3 + BDS2 + GPS combined POD.

3 POD model and processing strategy

3.1 BDS3 POD model

In POD, the satellite state vector at epoch t is expressed by the initial state at epoch t_0 and the state transition matrix. Therefore, the linearized equations for ionosphere-free (IF) code and carrier-phase observations are expressed as follows,

$$\begin{aligned} p_{r,\text{IF}}^s &= \psi_r^s \cdot (\Phi(t, t_0)^s \cdot \mathbf{o}_0^s - \mathbf{r}_r) - dt^s + dt_r \\ &\quad + c \cdot (d_{r,\text{IF}} - d_{\text{IF}}^s) + m_{r,\text{trop}} \cdot ZTD_r + e_{r,\text{IF}}^s \end{aligned} \quad (1)$$

$$\begin{aligned} l_{r,\text{IF}}^s &= \psi_r^s \cdot (\Phi(t, t_0)^s \cdot \mathbf{o}_0^s - \mathbf{r}_r) - dt^s + dt_r \\ &\quad + \lambda_{\text{IF}}(b_{r,\text{IF}} - b_{\text{IF}}^s + N_{r,\text{IF}}^s) \\ &\quad + m_{r,\text{trop}} \cdot ZTD_r + \varepsilon_{r,\text{IF}}^s \end{aligned} \quad (2)$$

$$\mathbf{o}_0^s = (x_0^s \ y_0^s \ z_0^s \ \dot{x}_0^s \ \dot{y}_0^s \ \dot{z}_0^s \ SRP_1^s \ SRP_2^s \cdots SRP_n^s)^T \quad (3)$$

where $p_{r,\text{IF}}^s$ and $l_{r,\text{IF}}^s$ denote “observed minus computed” (OMC) IF code and carrier-phase observations; ψ_r^s is the unit vector of the direction from receiver to satellite; \mathbf{r}_r is the increment vector of the receiver position; $\Phi(t, t_0)^s$ is state transition matrix from initial epoch t_0 to current epoch t ; \mathbf{o}_0^s is the initial orbit state vector of satellite s . dt^s and dt_r represent the clock biases for satellite and receiver, respectively. λ_{IF} is the wavelength of the IF carrier-phase, and $N_{r,\text{IF}}^s$ is the IF carrier-phase ambiguity; $b_{r,\text{IF}}$ and b_{IF}^s are the

IF receiver- and satellite-dependent phase delays (Ge et al. 2008; Li et al. 2011); $d_{r,IF}$ and d_{IF}^s are the IF code delay for receiver and satellite, and c is the speed of light. ZTD_r is the residual part of the zenith wet tropospheric delay, and $m_{r,trop}$ is the wet mapping function. $e_{r,IF}^s$ and $\varepsilon_{r,IF}^s$ are the sum of IF combination measurement noise and multipath for code and carrier phase, respectively. x_0^s , y_0^s and z_0^s are the satellite initial positions; \dot{x}_0^s , \dot{y}_0^s and \dot{z}_0^s are the satellite initial velocity; ($SRP_1^s SRP_2^s \cdots SRP_n^s$) are the Solar Radiation Pressure (SRP) parameters. For BDS triple-frequency code and carrier-phase observations, IF combinations can be formed by B1 + B2 (the linear combinations of B1 and B2) and B1 + B3 (the linear combinations of B1 and B3).

The IF code delays d_{IF}^s and $d_{r,IF}$ can be, respectively, absorbed into satellite and receiver clock bias, and the IF phase delays b_{IF}^s and $b_{r,IF}$ can be absorbed by the float IF ambiguity,

$$d\bar{t}_{IF}^s = dt^s + d_{IF}^s \quad (4)$$

$$d\bar{t}_{r,IF} = dt_r + d_{r,IF} \quad (5)$$

$$\bar{N}_{r,IF}^s = b_{r,IF} - b_{IF}^s + N_{r,IF}^s \quad (6)$$

Since both satellite and receiver clocks are unknown, one receiver clock bias is set to zero as reference clock. As a result, the estimated parameters in POD are expressed by

$$X = (\mathbf{o}_0^s \mathbf{r}_r d\bar{t}_{IF}^s d\bar{t}_{r,IF} ZTD_r \bar{N}_{r,IF}^s \delta_{eop})^T \quad (7)$$

where δ_{eop} is the Earth orientation parameters (EOP). When experimental BDS3, BDS2 and GPS are processed together, the linearized IF observations are expressed by Li et al. (2015)

$$\left\{ \begin{array}{l} p_{r,IF}^{C3} = \psi_r^{C3} \cdot (\Phi(t, t_0)^{C3} \cdot \mathbf{o}_0^{C3} - \mathbf{r}_r) - dt^{C3} + dt_r \\ \quad + c \cdot (d_{r,C3,IF} - d_{IF}^{C3}) + m_{r,trop} \cdot ZTD_r + e_{r,IF}^{C3} \\ p_{r,IF}^{C2} = \psi_r^{C2} \cdot (\Phi(t, t_0)^{C2} \cdot \mathbf{o}_0^{C2} - \mathbf{r}_r) - dt^{C2} + dt_r \\ \quad + c \cdot (d_{r,C2,IF} - d_{IF}^{C2}) + m_{r,trop} \cdot ZTD_r + e_{r,IF}^{C2} \\ p_{r,IF}^G = \psi_r^G \cdot (\Phi(t, t_0)^G \cdot \mathbf{o}_0^G - \mathbf{r}_r) - dt^G + dt_r \\ \quad + c \cdot (d_{r,G,IF} - d_{IF}^G) + m_{r,trop} \cdot ZTD_r + e_{r,IF}^G \end{array} \right. \quad (8)$$

$$\left\{ \begin{array}{l} l_{r,IF}^{C3} = \psi_r^{C3} \cdot (\Phi(t, t_0)^{C3} \cdot \mathbf{o}_0^{C3} - \mathbf{r}_r) - dt^{C3} + dt_r \\ \quad + \lambda_{IF,C3}(b_{r,C3,IF} - b_{IF}^{C3} + N_{r,IF}^{C3}) \\ \quad + m_{r,trop} \cdot ZTD_r + \varepsilon_{r,IF}^{C3} \\ l_{r,IF}^{C2} = \psi_r^{C2} \cdot (\Phi(t, t_0)^{C2} \cdot \mathbf{o}_0^{C2} - \mathbf{r}_r) - dt^{C2} + dt_r \\ \quad + \lambda_{IF,C2}(b_{r,C2,IF} - b_{IF}^{C2} + N_{r,IF}^{C2}) \\ \quad + m_{r,trop} \cdot ZTD_r + \varepsilon_{r,IF}^{C2} \\ l_{r,IF}^G = \psi_r^G \cdot (\Phi(t, t_0)^G \cdot \mathbf{o}_0^G - \mathbf{r}_r) - dt^G + dt_r \\ \quad + \lambda_{IF,G}(b_{r,G,IF} - b_{IF}^G + N_{r,IF}^G) \\ \quad + m_{r,trop} \cdot ZTD_r + \varepsilon_{r,IF}^G \end{array} \right. \quad (9)$$

where indices $C3$, $C2$ and G refer to experimental BDS3, BDS2 and GPS, respectively. The receiver-dependent code delays $d_{r,C2,IF}$ and $d_{r,G,IF}$ are different in one receiver, and this difference is called inter-system bias (ISB) between BDS2 and GPS (Li et al. 2015). Similarly, there also exists ISB between experimental BDS3 and GPS,

$$\left\{ \begin{array}{l} d\bar{t}_{r,G,IF} = dt_r + d_{r,G,IF} \\ d\bar{t}_{r,C2,IF} = dt_r + d_{r,C2,IF} = d\bar{t}_{r,G,IF} + ISB_{G_C2} \\ d\bar{t}_{r,C3,IF} = dt_r + d_{r,C3,IF} = d\bar{t}_{r,G,IF} + ISB_{G_C3} \end{array} \right. \quad (10)$$

$$\left\{ \begin{array}{l} \bar{N}_{r,IF}^G = b_{r,G,IF} - b_{IF}^G + N_{r,IF}^G \\ \bar{N}_{r,IF}^{C2} = b_{r,C2,IF} - b_{IF}^{C2} + N_{r,IF}^{C2} \\ \bar{N}_{r,IF}^{C3} = b_{r,C3,IF} - b_{IF}^{C3} + N_{r,IF}^{C3} \end{array} \right. \quad (11)$$

Consequently, the estimated parameters in BDS3 + BDS2 + GPS combined POD are

$$X = \left(\mathbf{o}_0^{C3} \mathbf{o}_0^{C2} \mathbf{o}_0^G \mathbf{r}_r d\bar{t}_{IF}^{C3} d\bar{t}_{IF}^{C2} d\bar{t}_{IF}^G ZTD_r \bar{N}_{r,IF}^{C2} \bar{N}_{r,IF}^{C3} \right. \\ \left. \bar{N}_{r,IF}^G \delta_{eop} d\bar{t}_{r,G,IF} ISB_{G_C2} ISB_{G_C3} \right)^T \quad (12)$$

In addition to a zero reference clock, the zero-mean conditions are introduced for BDS2 and BDS3 ISBs, that is, the sum of ISBs of all stations for a system (e.g., BDS2 or BDS3) is set to zero (Li et al. 2015),

$$\left\{ \begin{array}{l} ISB_{G_C2,r1} + ISB_{G_C2,r2} + \cdots + ISB_{G_C2,rn} = 0 \\ ISB_{G_C3,r1} + ISB_{G_C3,r2} + \cdots + ISB_{G_C3,rn} = 0 \end{array} \right. \quad (13)$$

However, it is not yet confirmed whether ISB_{G_C3} and ISB_{G_C2} are the same or not. This issue will be discussed in detail in 4.1. If ISB_{G_C3} and ISB_{G_C2} have the same value, there is only one ISB parameter ISB_{G_C} :

$$ISB_{G_C,r1} + ISB_{G_C,r2} + \cdots + ISB_{G_C,rn} = 0 \quad (14)$$

3.2 Processing strategy

The prior precisions of observations are set to 2 m and 2mm for raw code and carrier-phase observations, respectively. The weights of observations depend on elevation, and the cutoff elevation is set to 7 degrees. The arc length of POD is 72 h with 5-min sampling interval. For any two adjacent 3-day solutions shifted by one or 2 days, there are 48- or 24-h orbit overlap errors. In this study, the 24-h orbit overlap is used to validate the POD results. Other detailed information about observational models, dynamical models and estimated parameters can be found in Table 4.

In our POD processing, the nominal PCO values provided by the Operational Control Center (OCC) are used for BDS3 experimental satellites (listed in Table 5), while PCV values

Table 4 Observational models, dynamical models and estimated parameters for experimental BDS3 POD

Items	Models
Basic observables	BDS3/BDS2: B1I + B3I IF code and phase combination GPS: L1 + L2 IF code and phase combination
Sampling rate	300 s
Arc length	3 days
Elevation cutoff	7°
Weight for observations	Elevation dependent, 1 for E > 30°, otherwise $2^{\circ} \sin(E)$
Geopotential	EGM2008 model up to 12×12
N-body gravity	Sun, Moon, and other planets (JPL DE405)
Solar radiation	ECOM 5-parameter with no initial value (Beutler et al. 1994)
Attitude model	Yaw-steering mode for BDS3
Tide displacement	Solid Earth tide, pole tide, ocean tide
Relativity effect	Considered
Phase windup	Phase polarization effects applied
Atmospheric drag	Not considered
Satellite antenna PCO	GPS: Corrected; igs14.atx BDS2: Corrected; Suggested values by igs14.atx BDS3: Corrected; Suggested values by OCC
Satellite antenna PCV	GPS: Corrected; igs14.atx BDS2: ignored BDS3: ignored
Receiver antenna PCO and PCV	Corrections for GPS are used for BDS
Tropospheric delay	Corrected by Saastamoinen model; with GMF mapping function estimation of ZTD and ZTD gradients as piecewise constant; 2-h ZTD and 24-h gradients
Station coordinates	Estimated with tight constraint
Receiver clocks	Epoch-wise estimated as white noise; Constant ISBs
Satellite clocks	Epoch-wise estimated as white noise
Satellite state vector	Estimated
Phase ambiguities	Real constant for each ambiguity arc; DD AR for network solution
EOP parameters	Estimated

are ignored. It is worth noting that different PCO values were reported by Zhao et al. (2017) for C31 and C32. However, from our testing, the two sets of PCO values result only 1–2 cm orbit inconsistency in along-track, cross-track component

in terms of 24-h overlap RMS, while only several millimeters in radial component. For BDS2, PCO values from igs14.atx (<http://igs.org/pub/station/general/igs14.atx>) are applied for all frequencies of GEO, IGSO and MEO satellites, and PCVs are also ignored. For GPS, both PCOs and PCVs are corrected with igs14.atx antenna file. As for receiver-phase center, PCO/PCV corrections of GPS are used for BDS.

For most BDS2 IGSO and MEO satellites, their attitude modes switch between yaw-steering and orbit-normal, while BDS2 GEO satellites always maintain orbit-normal attitude. The attitude mode for BDS3 experimental satellites is still not clear, and it will be studied and confirmed in Sect. 6. Here, yaw-steering mode is used for experimental BDS3. ECOM 5-parameter model with no initial values is applied for SRP acceleration.

Because the new signals of BDS3 experimental satellites remain in the internal test stage, observations of old B1 and B3 frequencies were selected for the BDS POD in this study. To verify the feasibility and accuracy of POD with B1 and B3, we select all the 31 MGEX stations (shown as red triangles in Fig. 3) which can track B1, B2 and B3 simultaneously to perform BDS2 POD with B1 + B3 and B1 + B2 observations, respectively. Figure 4 shows the averaged RMS values of 24-h POD overlap in along-track, cross-track and radial components for BDS2 B1 + B3 and B1 + B2 modes. It can be seen that for most MEO and IGSO satellites, B1 + B3 POD and B1 + B2 POD achieve comparable overlap with the differences less than 1 cm.

Different strategies (as listed in Table 6) are designed to study several critical issues on BDS3 POD, including ISB between experimental BDS3 and BDS2, the combined POD of experimental BDS3 with BDS2 and GPS, different networks and ambiguities resolution. For the three ambiguity resolution strategies of GEO_F_BDS3_F, GEO_F_BDS3_X and GEO_X_BDS3_X, “F” means float and “X” means fixed. For example, GEO_F_BDS3_F means that the ambiguities of GEOs and experimental BDS3 are float, and GEO_X_BDS3_X means that the ambiguities of GEOs and experimental BDS3 are fixed to integers. In all the strategies, the double-differenced (DD) ambiguities of GPS and BDS2 IGSO/MEO satellites are fixed. Datasets of DOY001–230 2017 are processed.

4 POD for BDS3 experimental satellites

4.1 ISB between experimental BDS3 and BDS2

In order to perform BDS3 + BDS2 combined POD, it should be confirmed in advance whether ISB between experimental BDS3 and BDS2 exists or not. For the receivers that can track both experimental BDS3 and BDS2 signals, their clock biases can be obtained from BDS2 + GPS and BDS3 + GPS

Table 5 PCOs referred to CoM of BDS3 experimental satellites (provided by OCC)

Satellite	B1 (mm)			B2 (mm)			B3 (mm)		
	x	y	z	x	y	z	x	y	z
C31	-45.6	-298.6	2564.0	-45.5	-296.2	2117.9	-45.5	-302.7	2203.6
C32	-45.6	-298.6	2564.0	-46.5	-296.2	2117.9	-45.5	-302.7	2203.6
C33	-198.7	6.3	1511.0	-197.9	13.0	1088.9	-196.1	4.5	1251.9
C34	-202.3	8.1	1487.5	-230.1	5.0	1097.7	-199.9	6.2	1210.3

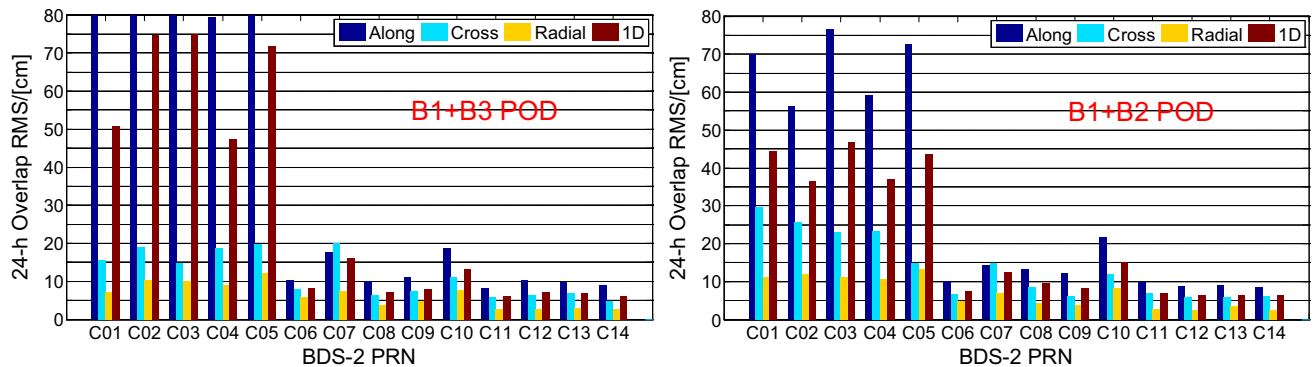


Fig. 4 24-h overlap RMS of BDS2 in B1 + B3 (left panel) and B1 + B2 (right panel) modes

Table 6 The strategies of BDS3 POD

Issue	Strategy (name)	System	BDS3 network
ISB between experimental BDS3 and BDS2	BDS3 + GPS	BDS3 + GPS	iGMAS + MGEX
BDS3 and BDS2	BDS2 + GPS	BDS2 + GPS	
Combined POD	BDS3-only	BDS3	iGMAS
	BDS3 + BDS2	BDS3 + BDS2	iGMAS
	BDS3 + BDS2 + GPS	BDS3 + BDS2 + GPS	iGMAS
Different networks	iGMAS-only	BDS3 + BDS2 + GPS	iGMAS
	MGEX-only		MGEX
	iGMAS + MGEX		iGMAS + MGEX
Ambiguity resolution	GEO_F_BDS3_F	BDS3 + BDS2 + GPS	iGMAS + MGEX
	GEO_F_BDS3_X		
	GEO_X_BDS3_X		

combined POD, respectively. The relationship of ISBs and receiver clock biases can be described as,

$$\begin{cases} d\bar{t}_{r,C3,IF} = d\bar{t}_{r,G,IF} + \text{ISB}_{r,G_C3} \\ d\bar{t}_{r,C2,IF} = d\bar{t}_{r,G,IF}' + \text{ISB}_{r,G_C2} \end{cases} \quad (15)$$

where $d\bar{t}_{r,G,IF}$ and $d\bar{t}_{r,G,IF}'$ are receiver clock biases for GPS from BDS3+GPS POD and BDS2+GPS POD, respectively; ISB_{r,G_C3} and ISB_{r,G_C2} are the ISBs of experimental BDS3 and BDS2 relative to GPS; $d\bar{t}_{r,C3,IF}$ and $d\bar{t}_{r,C2,IF}$ are receiver clock biases for experimental BDS3 and BDS2, respectively. Note that the receiver clock biases $d\bar{t}_{r,G,IF}$ and $d\bar{t}_{r,G,IF}'$ may differ to each other, because different receivers may be chosen as reference clock for BDS3+GPS and BDS2+GPS POD. To remove this bias, we choose

an iGMAS receiver (BJF1, for example) as reference clock, and the other receiver clocks are subtracted by the reference clock,

$$\begin{cases} \Delta d\bar{t}_{r,C3,IF} = d\bar{t}_{r,C3,IF} - d\bar{t}_{ref,C3,IF} \\ = (d\bar{t}_{r,G,IF} - d\bar{t}_{ref,G,IF}) \\ + (\text{ISB}_{r,G_C3} - \text{ISB}_{ref,G_C3}) \\ \Delta d\bar{t}_{r,C2,IF} = d\bar{t}_{r,C2,IF} - d\bar{t}_{ref,C2,IF} \\ = (d\bar{t}_{r,G,IF}' - d\bar{t}_{ref,G,IF}') \\ + (\text{ISB}_{r,G_C2} - \text{ISB}_{ref,G_C2}) \end{cases} \quad (16)$$

The difference between BDS2 and experimental BDS3 receiver clocks after removing reference clock can then be derived as:

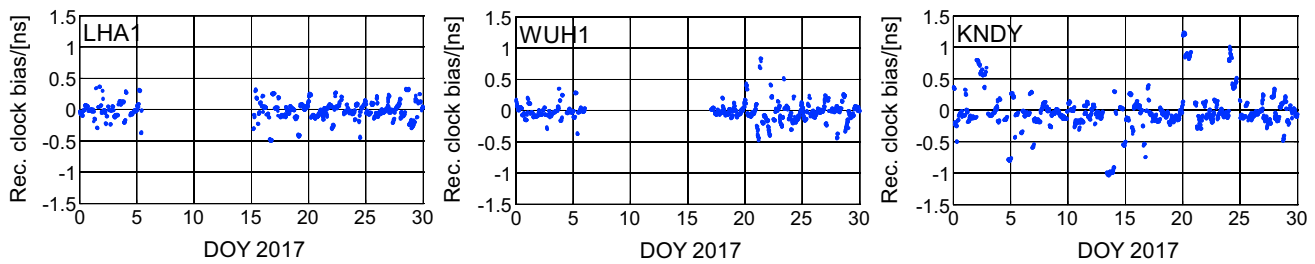


Fig. 5 Differences between experimental BDS3 and BDS2 receiver clocks after removing reference clock

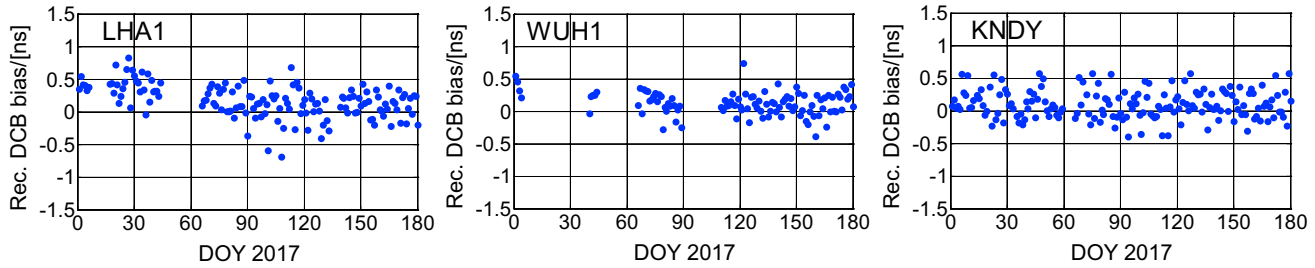


Fig. 6 Differences between experimental BDS3 and BDS2 receiver B1I–B3I DCBs

$$\Delta d\bar{t}_{r,C3,IF} - \Delta d\bar{t}_{r,C2,IF} = \text{ISB}_{r,C3,C2}^- \text{ISB}_{ref,C3,C2} \quad (17)$$

It means that the ISB difference between experimental BDS3 and BDS2 is equal to the differenced receiver clock between them. In Fig. 5, we present the results of clock difference $\Delta d\bar{t}_{r,C3,IF} - \Delta d\bar{t}_{r,C2,IF}$ at three iGMAS stations, which are mostly within ± 0.5 ns. The mean values are 0.013, 0.023 and 0.073 ns for LHA1, WUH1 and KNDY, respectively. No obvious systematic bias between experimental BDS3 and BDS2 is found.

We also estimate receiver DCBs for experimental BDS3 and BDS2, respectively. As only the B1I and B3I signals can be tracked simultaneously for experimental BDS3 and BDS2 satellites, the following analyses mainly focus on B1I–B3I DCB. The observation data from iGMAS/MGEX stations for DOY001–180, 2017 are processed to determine DCBs with the same strategy as Zhang et al. (2017b). The constraint that the sum of all satellite DCB values is zero is applied to separate the DCBs of satellites and receivers. The differences of experimental BDS3 and BDS2 receiver DCBs are plotted in Fig. 6. It can be found that the receiver DCBs of experimental BDS3 are in good agreement with those of BDS2, as the mean differences are within 0.15 ns.

The comparisons of both receiver clocks and the receiver DCBs demonstrate that no systematic bias between experimental BDS3 and BDS2 exists in the common B1I and B3I signals. As a consequence, only one ISB parameter needs to be estimated when performing BDS3 + BDS2 + GPS combined POD.

4.2 BDS3 + BDS2 + GPS combined POD

To evaluate the performance of BDS3-only POD and the contribution of multi-GNSS fusion to experimental BDS3 POD, the BDS3-only, BDS3 + BDS2, BDS3 + BDS2 + GPS POD strategies are evaluated with one-month data of DOY001–030 in 2017. Ten iGMAS stations (tracking experimental BDS3, BDS2 and GPS satellites) and 98 MGEX stations (tracking BDS2 and GPS satellites) are used here. The 24-h orbit overlap RMS values of four BDS3 experimental satellites are shown in Fig. 7. It can be found that the BDS3 + BDS2 + GPS combined POD strategy presents the smallest overlap, while the BDS3-only POD strategy performs the worst. For the BDS3 + BDS2 + GPS combined POD, the averaged 24-h overlap RMS values are 24.3, 16.1 and 8.4 cm in along-track, cross-track and radial components, respectively. The improvements are about 80–90% compared to BDS3-only POD and about 10% compared to BDS3 + BDS2 combined POD. It is easy to understand that the fusion of BDS2 and GPS improves the performance of BDS3 POD, because more satellites result in superior estimation of receiver clock offsets, troposphere parameters and station coordinates.

4.3 BDS3 POD with iGMAS + MGEX

To investigate the influence of tracking network on experimental BDS3 POD, observations from iGMAS and MGEX networks for DOY191–220, 2017 are processed. For this period, ten MGEX stations, equipped with SEPT POLARX5 receivers, are able to track the legacy B1I and B3I signals for experimental BDS3. In all the three strategies of

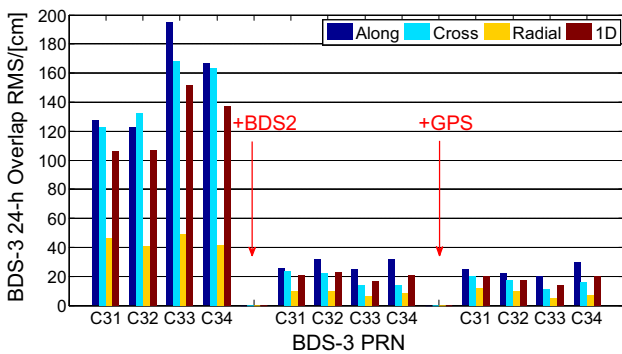


Fig. 7 24-h overlap of experimental BDS3 for BDS3-only, BDS3 + BDS2 and BDS3 + BDS2 + GPS POD

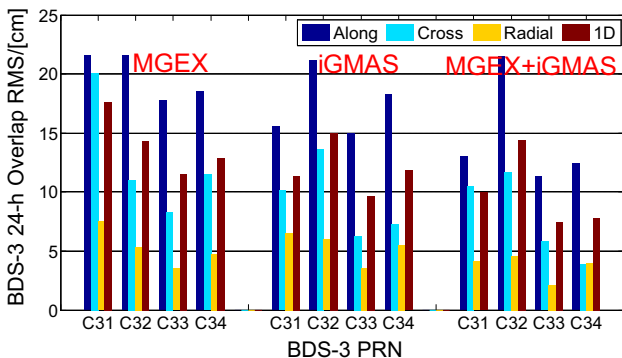


Fig. 8 24-h overlap of experimental BDS3 with different networks

iGMAS-only, MGEX-only and iGMAS + MGEX, experimental BDS3, BDS2 and GPS are combined together for POD.

The RMS values of 24-h orbit overlap for BDS3 experimental satellites are shown in Figure 8. It can be seen that with more observations, the iGMAS + MGEX strategy presents the smallest overlap of 14.6, 7.9 and 3.7 cm in along-track, cross-track and radial component, which is 25–40% better than MGEX-only and 15–30% better than iGMAS-only strategy. What's more, the POD performance with iGMAS network is slightly better than that with MGEX network. It may be attributed to the different geographic distributions of iGMAS and MGEX stations. We can also find that the POD performance of experimental BDS3 MEO/IGSO is comparable to that of BDS2, with slightly larger overlap RMS of 5–20%. This slightly larger overlap of experimental BDS3 is mainly caused by the fewer tracking stations compared to BDS2.

4.4 Influence of ambiguity resolution on POD

In order to evaluate the influence of ambiguity resolution (AR) on experimental BDS3 POD, one-month data of DOY191–220 in 2017 is processed with three ambiguity fixing strategies, including GEO_F_BDS3_F strategy (GEO

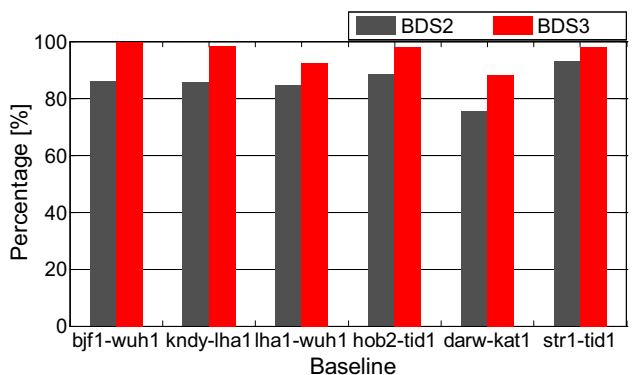


Fig. 9 Fixing rates of DD WL ambiguities at iGMAS and MGEX baselines

unfixed, experimental BDS3 unfixed), GEO_F_BDS3_X strategy (GEO unfixed, experimental BDS3 fixed) and GEO_X_BDS3_X strategy (GEO fixed, experimental BDS3 fixed), based on BDS3 + BDS2 + GPS combined POD. Twenty experimental BDS3 stations from both iGMAS and MGEX networks are used here.

The fixing rates of experimental BDS3 and BDS2 ambiguity are evaluated based on one-month data of six independent baselines. We assume that the ambiguity is fixed when the difference between the float ambiguity and its nearest integer is less than 0.15 cycles. As shown in Fig. 9, experimental BDS3 satellites present better double-differenced wide-lane (DD WL) fixing rates than that of BDS2 at all six baselines, with improvements of 4.72–13.79%. This may be attributed to the absence of satellite-induced code bias, which will affect DD WL AR. In experimental BDS3, the satellite-induced code bias is proved to be absent in observations (Zhang et al. 2017a), which would improve the fixing rates of DD WL AR particularly for long baselines. For BDS2, it is reported that the correction of satellite-induced code biases can significantly increase the fixing rates of DD WL AR (Geng et al. 2017). As for the double-differenced narrow-lane (DD NL) ambiguities, the fixing rate of experimental BDS3 is also 4.8–10.5% higher than that of BDS2. Figure 10 depicts the distribution of fractional parts of DD WL ambiguities. It can be found that the BDS3 experimental satellites present the best distribution of fractional parts of DD WL ambiguities, while BDS2 satellites show the worst. The RMS value of DD WL ambiguities is 0.093 cycles, which is 35.9% smaller than that of BDS2. However, the RMS value of DD NL ambiguities is nearly the same for experimental BDS3, BDS2 and GPS, which is about 0.15 cycles. The reason is that NL ambiguities are mainly determined from carrier-phase measurements, and the effect of the satellite-induced code bias on DD NL AR can be ignored.

Figure 11 shows 24-h orbit overlap RMS of BDS3 experimental satellites with different ambiguity fixing strategies. We can find that the GEO_F_BDS3_X strategy presents the

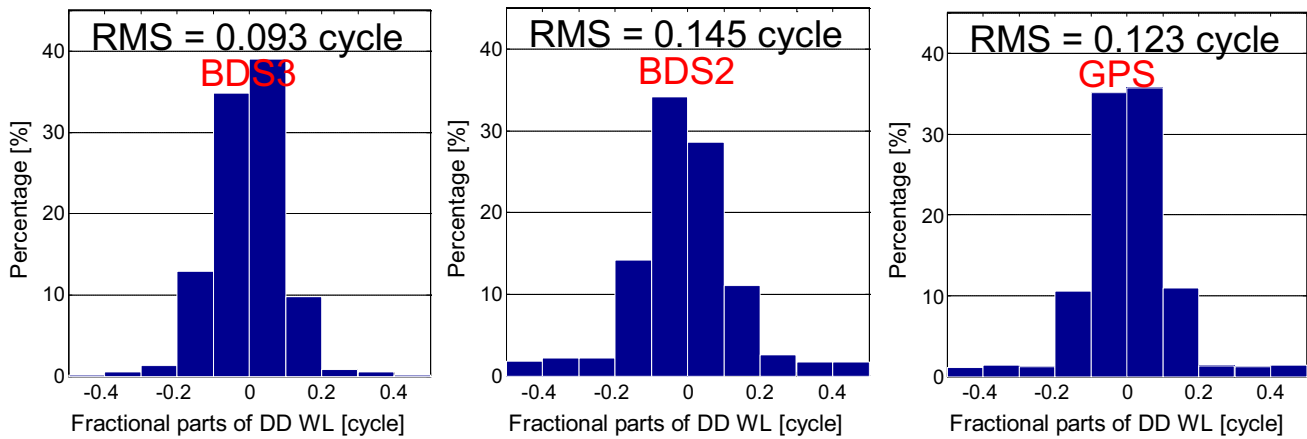


Fig. 10 Distribution histograms of fractional parts of DD WL ambiguities for experimental BDS3, BDS2 and GPS

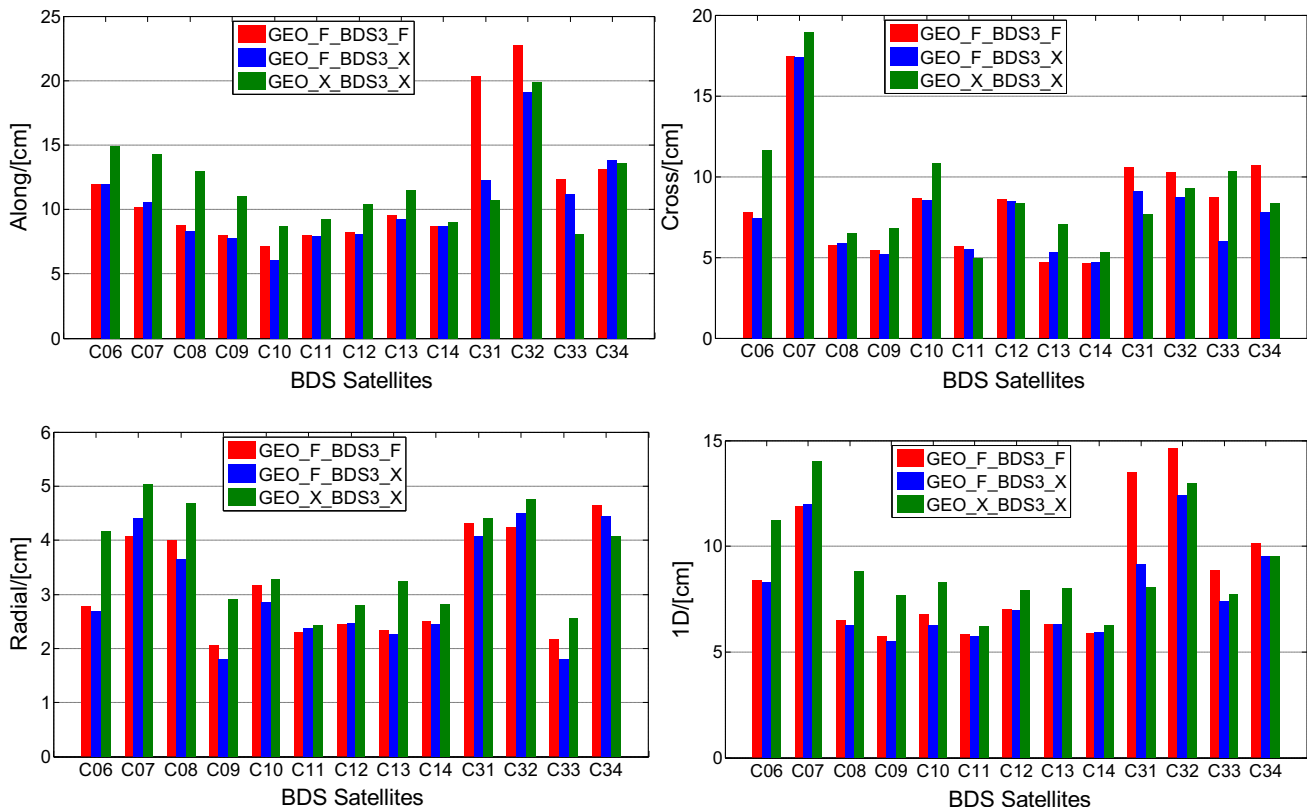


Fig. 11 24-h overlap of experimental BDS3 with three ambiguity fixing strategies

best performance for BDS3 POD, with RMS values being 14.6, 7.9 and 3.7 cm in along-track, cross-track and radial components. The improvements are 18.1, 21.3 and 6.5% compared to those of GEO_F_BDS3_F strategy. However, when the ambiguities of BDS2 GEO satellites are also fixed (GEO_X_BDS3_X strategy is applied), the overlap RMS of BDS3 POD gets larger, with increments of 12.6 and 10.4% in cross and radial components. The solution strength of GEO satellites is rather weak. The GEO float ambiguities are not

accurate enough and will be difficult to be fixed correctly. The POD performance will get worse once some GEO ambiguities are fixed to wrong integers.

As for the BDS2 satellites, the fixing of BDS3 ambiguities almost has no influence on BDS2 POD. But it can be noticed that GEO_X_BDS3_X strategy presents the worst performance for BDS2 POD compared with GEO_F_BDS3_F and GEO_F_BDS3_X strategies. In conclusion, for both experimental BDS3 and BDS2 satellites, the GEO_F_BDS3_X

Table 7 SLR offsets for experimental BDS3 satellites

Offset	C31	C32	C33	C34
X/mm	-959.1	185.1	612.1	610.1
Y/mm	181.3	685.4	-71.7	-71.2
Z/mm	637.6	1960.2	1229.0	1244.8

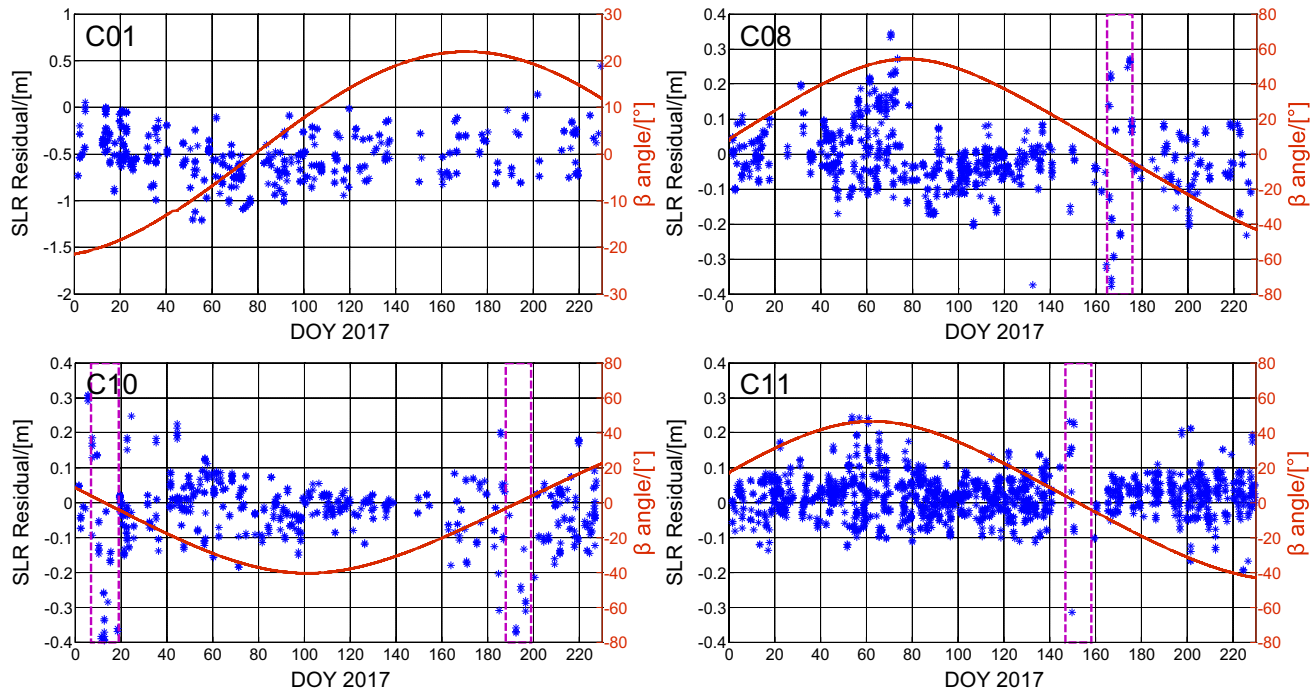
strategy can achieve the best performance, which will be applied in our following discussion.

5 Validations with SLR

Satellite Laser Ranging (SLR) is an optical technique for independent orbit validation. The laser ranging distances are compared with that computed by POD results, to identify whether systematic biases exist in POD results or not (Montenbruck et al. 2013; Hackel et al. 2015; Guo et al. 2016a). All BDS satellites are equipped with laser retroreflector arrays (LRAs). However, only C01, C08, C10, C11, C13, C32, C33 and C34 are tracked by the International Laser Ranging Service (ILRS) network during the study period (ftp://cds.gsfc.nasa.gov/pub/slrf/data/npt_crd). The LRA offset values for C01, C08, C10 and C11 are summarized by Montenbruck et al. (2015). For experimental BDS3, the LRA offsets suggested by OCC are listed in Table 7. Only the middle day of each 3-day POD solution is validated with SLR.

Figure 12 shows the SLR residuals of BDS2 POD results for DOY001-230 in 2017. The satellite attitude mode in the marked periods is ON, and significant SLR residual changes are observed during these periods. We can note that C01 satellite performs worst and has a systematic bias of -52.93 cm. In addition, the performance of C11 is better than that of C01, C08 and C10, which is possibly attributed to the better geometry condition of MEO satellites.

Furthermore, the SLR residuals of experimental BDS3 C32, C33 and C34 satellites are given in Fig. 13. The scatter and variation for experimental BDS3 appear notably larger than those for BDS2, which may be attributed to the smaller network tracking experimental BDS3. The marked periods are also ON mode (if experimental BDS3 adopts the same attitude control mode as BDS2). However, the SLR residuals show no significant changes in these periods. After detection and removal of outliers in the SLR observations, there are 308 normal points (NP) available for C32, 275 for C33 and 334 for C34. The mean values are -3.48, 7.81 and 8.19 cm for C32, C33 and C34, respectively. The STD values are 13.35 cm for C32, 13.46 cm for C33 and 13.11 cm for C34. We can find that, for C33 and C34 satellites, the mean values are slightly worse than that of C32. These systematic variations are possibly caused by the inaccuracy of satellite PCOs and LRA offsets and/or the deficiencies of ECOM solar radiation pressure model. It is noted that some of the experimental BDS3 satellites are reported to have elongated shapes (Zhao et al. 2017). The 5-parameter ECOM model is not appropriate enough for the SRP modeling of these satellites, and a

**Fig. 12** SLR residuals of BDS2 C01, C08, C10 and C11 satellites against β angle

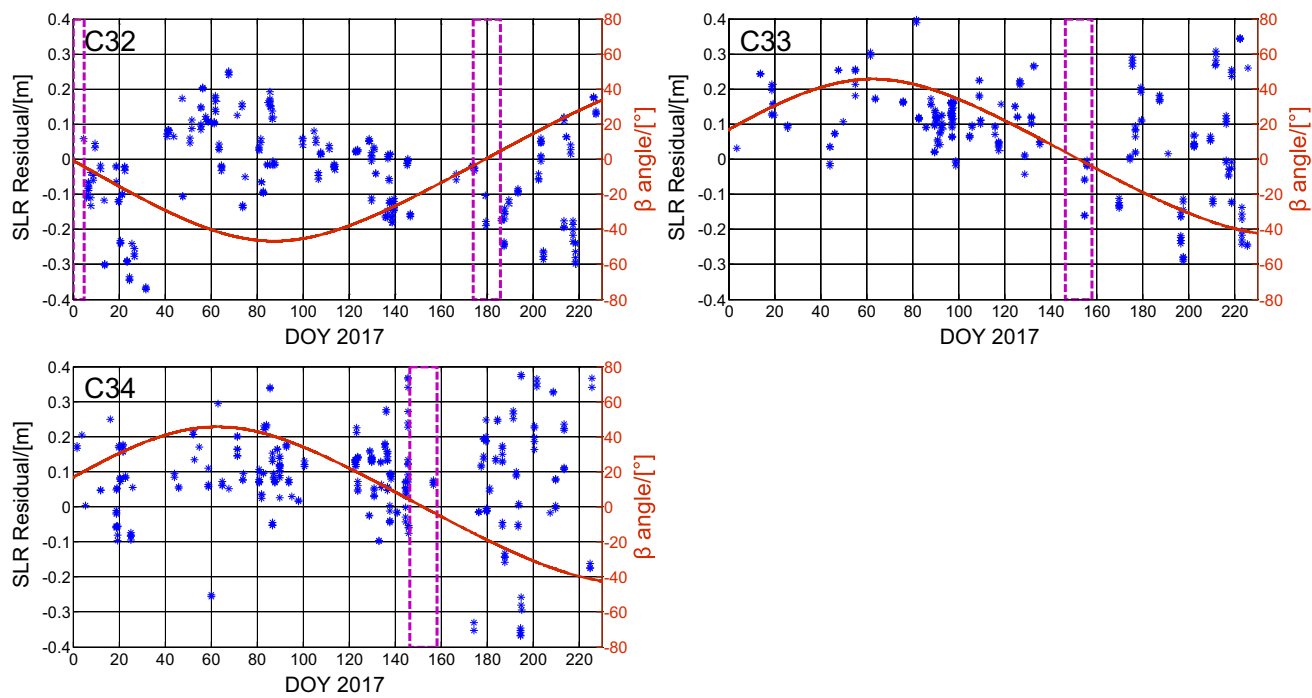


Fig. 13 SLR residuals of experimental BDS3 C32, C33 and C34 satellites against β angle

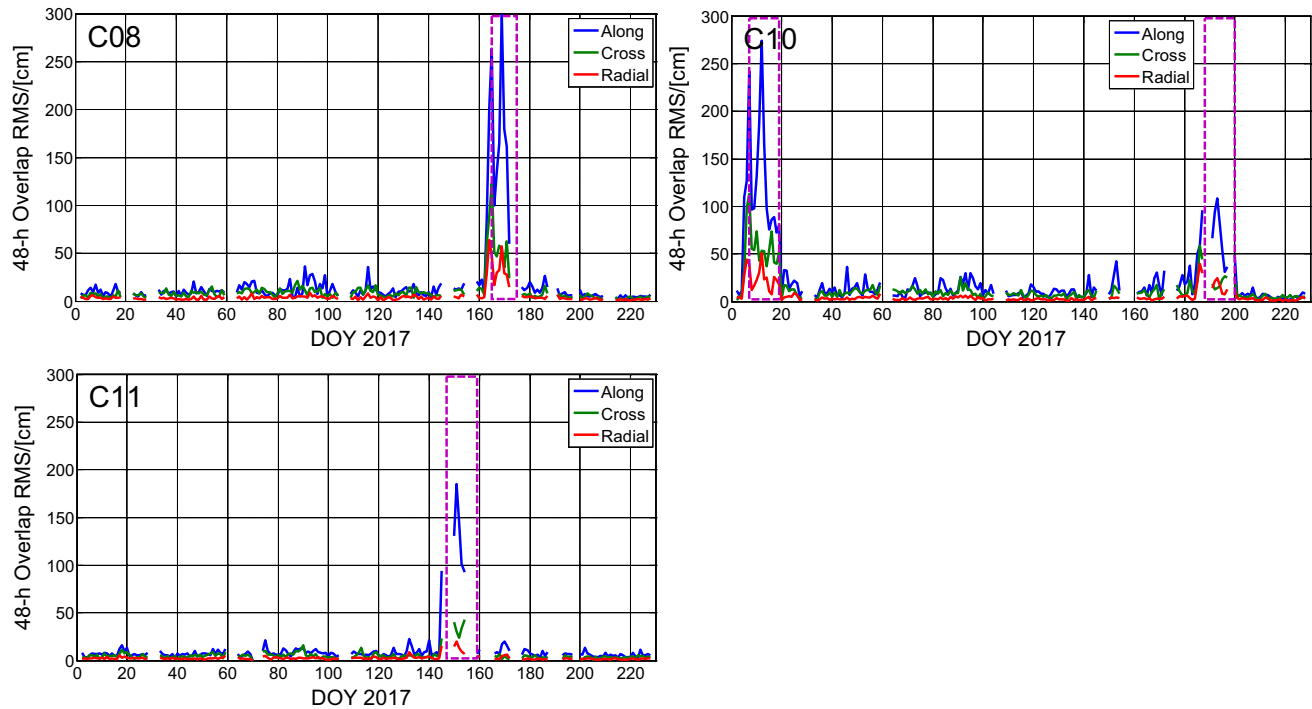


Fig. 14 The long-term variation of 48-h overlap RMS of BDS2 C08, C10 and C11 satellites

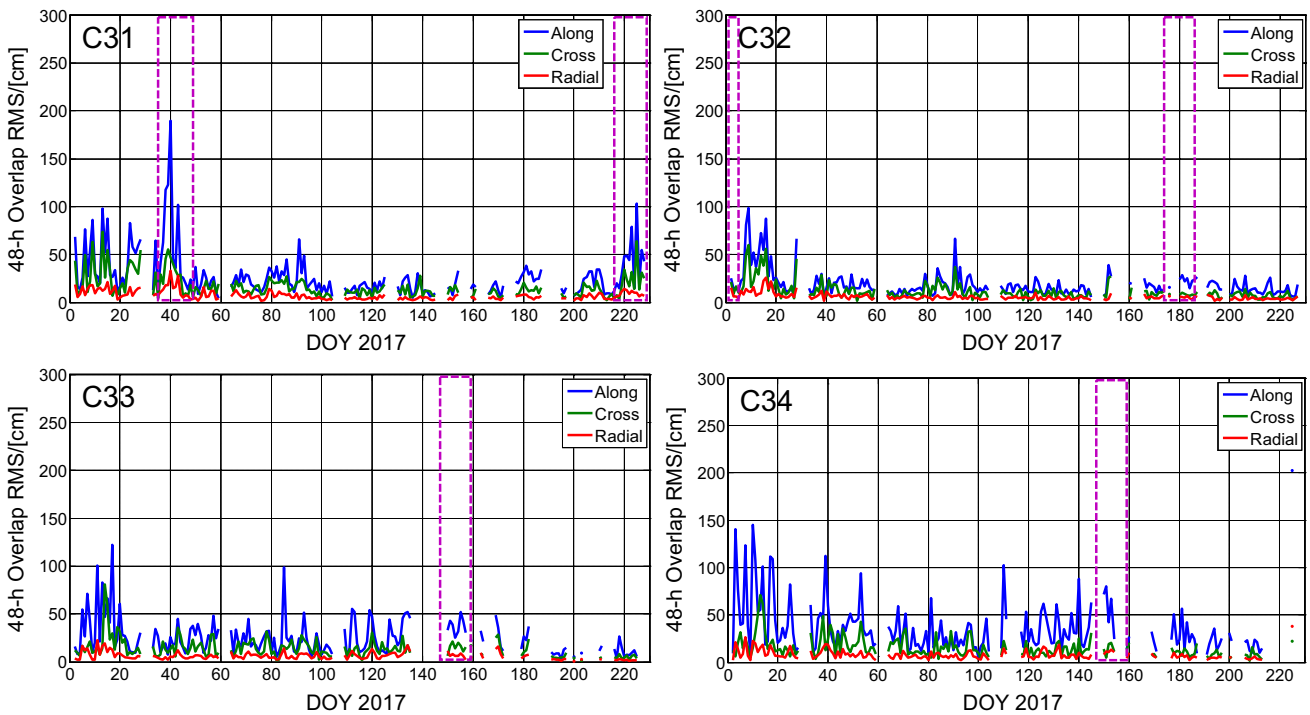


Fig. 15 The long-term variation of 48-h overlap RMS of experimental BDS3 C31, C32, C33 and C34 satellites

box-wing SRP model for experimental BDS3 C32 has been reported by Wang et al. (2018).

6 Attitude of BDS3 experimental satellites

According to the discussion in Sect. 5, the SLR residuals of BDS2 satellites change significantly during ON mode, while this phenomenon is not found in experimental BDS3 satellites. Due to limited normal points of SLR, 48-h overlap of DOY001-230 in 2017, as shown in Figs. 14 and 15, is further investigated in this section. During ON periods, significant increases in RMS can be seen in BDS2 IGSO (C08 and C10) and MEO (C11) satellites. However, for experimental BDS3 C32, C33 and C34, there are no obvious increases in the RMS values during ON period. However, the overlap of C31 presents increases in RMS during ON periods, which is similar to BDS2 satellites. According to Zhang et al. (2017a), C31 is not capable of transmitting new B1C, B2a and B2b signals but only B1I and B3I signals. It is possible that C31 adopts the same attitude control mode as BDS2, which needs further confirmation with OCC.

7 Conclusions

In this contribution, POD for BDS3 experimental satellites is studied using iGMAS and MGEX networks. Data of 230

days from DOY001-230, 2017 are processed with different strategies to study several critical issues in detail, including ISB between experimental BDS3 and BDS2, experimental BDS3 POD with different networks, ambiguity resolution, and the attitude mode of BDS3 experimental satellites.

The ISB between experimental BDS3 and BDS2 is analyzed by the differences of receiver clock biases and receiver DCBs. The averaged differences of receiver clocks between experimental BDS3 and BDS2 are 0.013, 0.023 and 0.073 ns at LHA1, WHU1 and KNDY, and the receiver B1I-B3I DCBs of experimental BDS3 and BDS2 are in good agreement. The nearly zero differences of receiver clocks and DCBs confirm that no obvious systematic bias between experimental BDS3 and BDS2 exists in the common B1I and B3I signals. As a result, experimental BDS3 and BDS2 can be treated as one system in combined POD. The fusion with BDS2 and GPS can improve the performance of experimental BDS3, and the 24-h overlap RMS of BDS3+BDS2+GPS combined POD is 24.3, 16.1, and 8.4 cm in along-track, cross-track and radial components, when only 10 iGMAS stations are used. The POD performance with 10 MGEX-only stations is slightly worse than that with iGMAS-only network, which may be attributed to the different geographic distributions of iGMAS and MGEX stations. With iGMAS + MGEX observations, experimental BDS3 POD achieves a smaller 24-h overlap of 14.6, 7.9 and 3.7 cm, which is still slightly larger than that of BDS2 IGSO/MEO due to the fewer BDS3 tracking stations.

Different ambiguity resolution strategies, namely GEO_F_BDS3_F, GEO_F_BDS3_X, GEO_X_BDS3_X, are applied for experimental BDS3 POD. The best performance is achieved with GEO_F_BDS3_X. The wrong fixing of GEO-related ambiguities may lead to decreasing POD performance. In addition, experimental BDS3 presents higher DD WL ambiguity fixing rates than BDS2. The fractional parts of DD WL ambiguities of experimental BDS3 also show better distribution and smaller RMS than that of BDS2. This may be attributed to the absence of satellite-induced bias. The 230-day SLR validation is performed, and the mean values are -3.48 , 7.81 and 8.19 cm for C32, C33 and C34, respectively, with STD of 13.35 , 13.46 and 13.11 cm. The long-term orbit overlap comparisons show that C31 most likely still uses an orbit-normal mode and exhibits similar orbit modeling problems as found in most of the BDS2 satellites, which needs further investigation.

Acknowledgements We are grateful to iGMAS and IGS-MGEX for providing multi-GNSS data and products. Thanks also go to the EPOS-RT/PANDA software provided by GFZ. This study was financially supported by the National Natural Science Foundation of China (Grant No. 41774030).

References

- Beutler G, Brockmann E, Gurtner W et al (1994) Extended orbit modeling techniques at the CODE processing center of the international GPS service for geodynamics (IGS): theory and initial results. *Manuscripta Geodaetica* 19:367–386
- Cai H, Chen G, Jiao W et al (2016) An initial analysis and assessment on final products of iGMAS. In: Sun J, Liu J, Fan S, Wang F (eds) China satellite navigation conference (CSNC) 2016 proceedings: volume III. Lecture notes in electrical engineering, vol 390. Springer, Singapore
- CSNO (2017) BeiDou navigation satellite system signal in space interface control document B1C and B2a open service signal (test version). China Satellite Navigation Office
- CSNO (2018) BeiDou navigation satellite system signal in space interface control document open service signal B3I (version 1.0). China Satellite Navigation Office
- Dai X, Ge M, Lou Y et al (2015) Estimating the yaw-attitude of BDS IGSO and MEO satellites. *J Geod* 89:1005–1018. <https://doi.org/10.1007/s00190-015-0829-x>
- Ge M, Gendi G, Rothacher M et al (2008) Resolution of GPS carrier-phase ambiguities in Precise Point Positioning with daily observations. *J Geod* 82(7):389–399
- Geng T, Xie X, Zhao Q et al (2017) Improving BDS integer ambiguity resolution using satellite-induced code bias correction for precise orbit determination. *GPS Solut*. <https://doi.org/10.1007/s10291-017-0602-0>
- Guo F, Li X, Zhang X et al (2016a) Assessment of precise orbit and clock products for Galileo, BeiDou, and QZSS from IGS Multi-GNSS Experiment (MGEX). *GPS Solut* 21:279–290. <https://doi.org/10.1007/s10291-016-0523-3>
- Guo J (2014) The impacts of attitude, solar radiation and function model on precise orbit determination for GNSS satellites. PhD dissertation (in Chinese with English abstract), GNSS Research Center, Wuhan University, Wuhan
- Guo J, Chen G, Zhao Q et al (2017) Comparison of solar radiation pressure models for BDS IGSO and MEO satellites with emphasis on improving orbit quality. *GPS Solut* 21:511–522. <https://doi.org/10.1007/s10291-016-0540-2>
- Guo J, Xu X, Zhao Q et al (2016b) Precise orbit determination for quad-constellation satellites at Wuhan University: strategy, result validation, and comparison. *J Geod* 90:143–159. <https://doi.org/10.1007/s00190-015-0862-9>
- Hackel S, Steigenberger P, Hugentobler U et al (2015) Galileo orbit determination using combined GNSS and SLR observations. *GPS Solut* 19(1):15–25. <https://doi.org/10.1007/s10291-013-0361-5>
- He L, Ge M, Wang J et al (2013) Experimental study on the precise orbit determination of the BeiDou navigation satellite system. *Sensors* 13(3):2911–2928. <https://doi.org/10.3390/s130302911>
- Kaplan ED, Hegarty C (2017) Understanding GPS/GNSS: principles and applications, 3rd edn. Artech House, Norwood
- Li X, Ge M, Dai X et al (2015) Accuracy and reliability of multi-GNSS real-time precise positioning: GPS, GLONASS, BeiDou, and Galileo. *J Geod* 89(6):607–635
- Li X, Li X, Yuan Y et al (2017) Multi-GNSS phase delay estimation and PPP ambiguity resolution: GPS, BDS, GLONASS, Galileo. *J Geod* <https://doi.org/10.1007/s00190-017-1081-3>
- Li X, Zhang X, Ge M (2011) Regional reference network augmented precise point positioning for instantaneous ambiguity resolution. *J Geod* 85:151–158
- Lou Y, Liu Y, Shi C et al (2014) Precise orbit determination of BeiDou constellation based on BETS and MGEX network. *Sci Rep* 4:4692. <https://doi.org/10.1038/srep04692>
- Lou Y, Liu Y, Shi C et al (2016) Precise orbit determination of BeiDou constellation: method comparison. *GPS Solut* 20:259–268. <https://doi.org/10.1007/s10291-014-0436-y>
- Montenbruck O, Schmid R, Schmid R et al (2015) GNSS satellite geometry and attitude models. *Adv Space Res* 56:1015–1029
- Montenbruck O, Steigenberger P, Prange L et al (2017) The multi-GNSS experiment (MGEX) of the international GNSS service (IGS)—achievements, prospects and challenges. *Adv Space Res* 59:1671–1697
- Montenbruck O, Steigenberger P, Kirchner G (2013) GNSS satellite orbit validation using satellite laser ranging. In: ILRS workshop proceedings, vol 16, pp 1095–1095
- SCIO (2016) China's BeiDou navigation satellite system by the state council information office of the People's Republic of China (SCIO). Foreign Languages Press. June 2016. [http://www.beidou.gov.cn/attach/beidou/China's%20BeiDou%20Navigation%20Satellite%20System\(English\).pdf](http://www.beidou.gov.cn/attach/beidou/China's%20BeiDou%20Navigation%20Satellite%20System(English).pdf). Accessed 11 Mar 2017
- Shi C, Zhao Q, Li M et al (2012) Precise orbit determination of Beidou satellites with precise positioning. *Sci China Earth Sci* 55(7):1079–1086. <https://doi.org/10.1007/s11430-012-4446-8>
- Steigenberger P, Hugentobler U, Hauschild A, Montenbruck O (2013) Orbit and clock analysis of compass GEO and IGSO satellites. *J Geod* 87(6):515–525. <https://doi.org/10.1007/s00190-013-0625-4>
- Tan B, Yuan Y, Wen M et al (2016) Initial results of the precise orbit determination for the new-generation BeiDou satellites (BeiDou-3) based on the iGMAS network. *ISPRS Int J Geo Inf* 5(12):196
- Wang C, Guo J, Zhao Q et al (2018) Solar radiation pressure models for BeiDou-3 I2-S satellite: comparison and augmentation. *Remote Sens* 10(1):118. <https://doi.org/10.3390/rs10010118>
- Wanninger L, Beer S (2015) BeiDou satellite-induced code pseudorange variations: diagnosis and therapy. *GPS Solut* 19(4):639–648
- Xie X, Geng T, Zhao Q et al (2017) Performance of BDS-3: measurement quality analysis, precise orbit and clock determination. *Sensors* 17(6):1233
- Yang Y, Tang J, Montenbruck O (2017) Chinese navigation satellite systems. In: Teunissen PJG, Montenbruck O (eds) Springer Hand-

- book of global navigation satellite systems. Springer, Berlin, pp 273–304
- Zhang R, Zhang Q, Huang G et al (2015) Impact of tracking station distribution structure on BeiDou satellite orbit determination. *Adv Space Res* 56(10):2177–2187. <https://doi.org/10.1016/j.asr.2015.07.045>
- Zhang X, Wu M, Liu W et al (2017a) Initial assessment of the COMPASS/BeiDou-3: new-generation navigation signals. *J Geod.* <https://doi.org/10.1007/s00190-017-1020-3>
- Zhang X, Xie W, Ren X et al (2017b) Influence of the GLONASS inter-frequency bias on differential code bias estimation and ionospheric modeling. *GPS Solut* 21(3):1355–1367
- Zhao Q, Guo J, Li M et al (2013) Initial results of precise orbit and clock determination for COMPASS navigation satellite system. *J Geod* 87(5):475–486. <https://doi.org/10.1007/s00190-013-0622-7>
- Zhao Q, Wang C, Guo J et al (2017) Precise orbit and clock determination for BeiDou-3 experimental satellites with yaw attitude analysis. *GPS Solut* 22:4. <https://doi.org/10.1007/s10291-017-0673-y>